IEEE Access
Multidisciplinary | Rapid Review | Open Access Journal

Received September 5, 2021, accepted September 20, 2021, date of publication October 5, 2021, date of current version October 14, 2021.

Digital Object Identifier 10.1109/ACCESS.2021.3118076

Prediction of Cerebral Palsy in Newborns With Hypoxic-Ischemic Encephalopathy Using Multivariate EEG Analysis and Machine Learning

DALAL BAKHEET[1,2], NOURA ALOTAIBI[1,2], DANIEL KONN[3], BRIGITTE VOLLMER[4,5], AND KOUSHIK MAHARATNA[1], (Member, IEEE)

[1]School of Electronics and Computer Science, University of Southampton, Southampton SO17 1BJ, U.K.
[2]Computer Science and Artificial Intelligence Department, University of Jeddah, Jeddah 21959, Saudi Arabia
[3]Clinical Neurophysiology, University Hospital Southampton, Southampton SO16 6YD, U.K.
[4]Clinical Neurosciences, Clinical and Experimental Sciences, Faculty of Medicine, University of Southampton, Southampton SO16 6YD, U.K.
[5]Paediatric Neurology, Southampton Children's Hospital, Southampton SO16 6YD, U.K.

Corresponding author: Dalal Bakheet (dmb1y17@soton.ac.uk)

This work was supported in part by the Scholarship Program of the University of Jeddah, Jeddah, Saudi Arabia.

This work involved human subjects or animals in its research. Approval of all ethical and experimental procedures and protocols was granted by the HRA and Health and Care Research Wales (HCRW) under reference ID 20/HRA/0260, IRAS project ID 278072, and University Hospital Southampton Research and Development protocol number RHM CHI1047.

ABSTRACT This study was carried out to investigate whether the quantitative analysis of electroencephalogram (EEG) signals of infants with hypoxic-ischemic encephalopathy (HIE) can be used for early prediction of cerebral palsy (CP). We computed sample entropy (SampEn), permutation entropy (PEn), and spectral entropy (SpEn) measures to reflect the signals' complexity and the graph-theoretic parameters derived from weighted phase-lag index (WPLI) to measure functional brain connectivity. Both feature sets were calculated in the noise-assisted multivariate empirical mode decomposition (NA-MEMD) domain to characterize the tempo-spectral integration of information and thus provide novel insight into the brain dynamics. Statistical analysis results showed a general abnormality in the EEG of individuals with CP at the alpha-band component. Particularly, complexity measures were decreased, and graph-theoretic parameters specified by the diameter feature were increased in infants with CP compared to those with normal neurology. The proposed set of features have also been evaluated using the random under-sampling boosting (RUSBoost) classifier, which was trained and tested on the feature vectors of a cohort of 26 infants - 6 who developed CP by the age of 24 months and 20 with normal neuromotor outcome. A good performance of 84.6% classification accuracy (ACC), 83% sensitivity (SNS), 85% specificity (SPC) and 0.87 area under curve (AUC) was obtained using the entropy features extracted from the alpha-band component. A close result of 80.8% ACC, 67% SNS, 85% SPC and 0.79 AUC was also achieved using the diameter feature calculated from the same frequency range. Therefore, it was concluded that the obtained brain functions' characteristics successfully discriminate between the two groups of infants. These characteristics could be considered potential biomarkers of cerebral cellular damage and, therefore, could be employed in practical clinical applications for early CP prediction.

INDEX TERMS Brain connectivity, cerebral palsy (CP), electroencephalogram (EEG), empirical mode decomposition (EMD), hypoxic-ischemic encephalopathy (HIE), graph theory, noise-assisted multivariate empirical mode decomposition (NA-MEMD), weighted phase-lag index (WPLI).

The associate editor coordinating the review of this manuscript and approving it for publication was Hasan S. Mir.

I. INTRODUCTION

Hypoxic-ischemic encephalopathy (HIE) as a consequence of perinatal asphyxia is one of the common causes of neonatal

brain injury. Subsequent neuromotor impairment – cerebral palsy (CP) [1] - remains a frequent outcome, even when infants are treated with hypothermia, which is now standard clinical care in most centers. CP is a movement and posture disorder frequently associated with epilepsy, impairment of sensation, cognition, communication, and/or behavior [2]. As a lifelong condition, it has a severe socio-economic impact on families and health care systems [3]. Early identification of infants with neonatal HIE who are at high risk of developing CP later in life is important for appropriate early counseling and planning of intervention strategies [4], which ultimately may lead to improved outcomes.

Hadders-Algra [4] has provided a detailed review of the opportunities and challenges for early diagnosis and early intervention in CP. This review concluded that the most frequently used assessment methods for early prediction of CP are (a) neurological and neuromotor assessments, (b) neuroimaging, and (c) neurophysiological tests. Even though neurological and neuromotor assessments have been widely used in diagnosing CP and their prediction value is generally good, they are subjective and often require a longitudinal series of tests to detect the abnormalities.

Alternatively, neuroimaging techniques have been used as promising tools for the early prediction of CP in high-risk infants [4], and magnetic resonance imaging (MRI) is the preferred imaging technique for this purpose [5]–[11]. Moreover, considerable literature employed neurophysiological tests with infants at risk of adverse neurodevelopmental outcomes. Conventional grading electroencephalogram (cEEG) and amplitude-integrated electroencephalogram (aEEG) modalities were found to predict the outcome well [5], [10]–[13]. However, interpretation of the prognostic value of these methods remains subjective [14].

On the other hand, quantitative EEG (qEEG) analysis could provide objective, reproducible and reliable biomarkers to characterize the brain activities related to CP. These measures have been suggested to be the gold standard biomarker for identifying CP.

Spectral power, functional brain connectivity, particularly coherence, and complexity analysis of EEG signals are the most common features used in this field. Gao *et al.* [15], [16] employed linear-complexity measures to assess the temporal and spatial correlations of EEG signals in adolescent patients with CP and their neurotypical peers. Nevertheless, EEG is a nonlinear and non-stationary signal in nature [17], and such linear-based measurements are not well adapted for its analysis.

Coherence measures and spectral power were employed in different studies, such as [18]–[20], to characterize EEG signals of children with CP. However, coherence measures are significantly affected by the volume conduction issue [15]. Moreover, coherence is further restricted by its assumption of the linearity of the signal and its low temporal resolution. On the other hand, spectral power-based measures are often limited by their stationarity assumption of signals and their reliance on the predefined traditional brain waves. Prior selection of the frequency ranges may lead to omitting potentially meaningful brain dynamics, specifically in the case of infants, due to the well-known variability between them and the older individuals in the neural oscillations of interest [21].

Details on the CP identification using nonlinear complexity analysis are limited to Sajedi *et al.* [22], who employed a fractal dimension to measure the nonlinear complexity of EEGs. Nevertheless, they estimated the fractal dimension from broad-band EEGs and did not consider the series of different intrinsic oscillations inherent in the signals [17].

Thus, although different qEEG research has been conducted to explore the brain activities related to CP, no single study exists that employed a qEEG measure that considers the nonlinearity and nonstationary characteristics of EEG. Furthermore, all previous studies have been carried out in adolescents and children with CP, and the detailed exploration of using qEEG to identify CP at infancy was rarely investigated [23].

Therefore, this research aims to investigate the effectiveness of two qEEG approaches in a machine learning framework for early prediction of CP in term-born infants with neonatal HIE, diagnosed as having CP or no CP at 24 months of age. Functional brain connectivity, specifically weighted phase lag-index (WPLI) characterized by graph-theoretical parameters, and complexity analysis of EEG utilizing sample entropy (SampEn), permutation entropy (PEn), and spectral entropy (SpEn), are the two methods proposed in this study to characterize infants' resting-state EEG. Both approaches consider the nonlinearity and nonstationarity nature of EEG signals. Further, the WPLI connectivity measure is robust against the volume conduction issue, mainly raised with the coherence measures used in the literature. These measures have been successfully used in diagnosing various brain disorders [24], [25].

The fundamental difference between WPLI and complexity measures is that the functional brain connectivity characterizes the interaction between different brain areas over time, while the entropies reflect the complex behavior of each EEG signal independently.

Noise-assisted multivariate empirical mode decomposition (NA-MEMD) has been utilized to adaptively decompose (without *a priori* selection of the filter cut-offs) the EEG signal into finite oscillation scales at the time domain. The proposed two sets of features were then computed from each scale to characterize the overlapping time-frequency brain dynamics associated with CP.

Statistical analysis was initially utilized to evaluate the capability of the entropies and WPLI-based measures in discriminating between infants with CP and infants with normal neurology. The features were then used to train and test a random under-sampling boosting (RUSBoost) classifier to show how useful they could be in practical CP prediction. The whole proposed methodology is depicted in Fig. 1.

The rest of the paper is structured as follows: Section II describes the materials and methods adopted here.

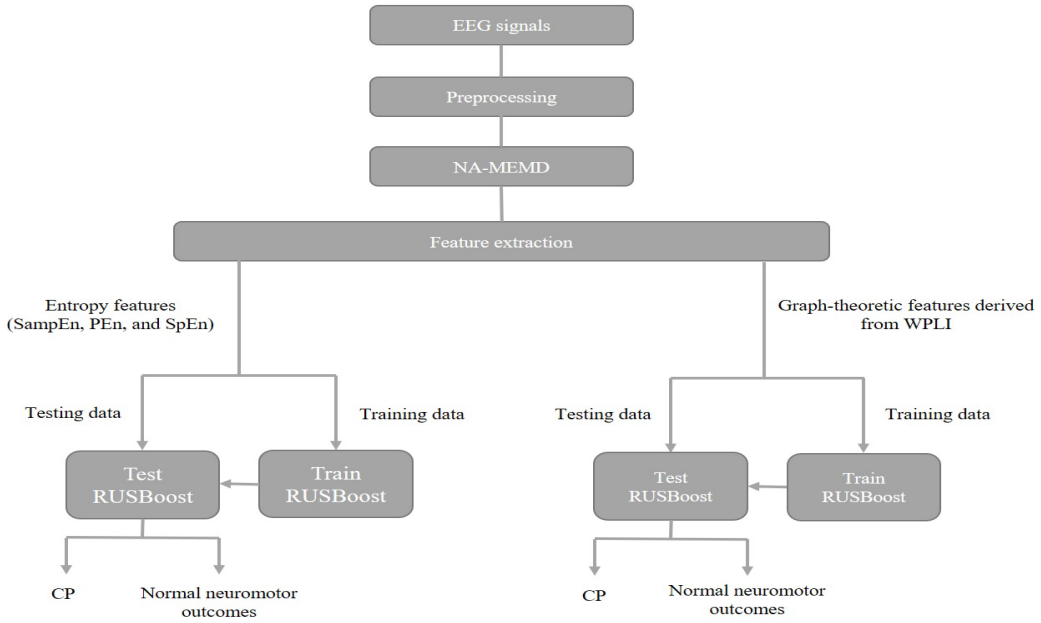

FIGURE 1. Block diagram of the proposed methodology for the classification of infants with CP and infants with normal neurology.

The analysis results are presented in Section III and discussed in detail in Section IV. Section V concludes the paper and suggests some future research directions.

II. MATERIALS AND METHODS

This section describes the experimental data and the employed preprocessing methods used to generate artefact-free EEG. It then reviews the NA-MEMD decomposition method as well as the complexity and WPLI-based measures. The proposed feature extraction schemes, statistical analysis method and the RUSBoost classifier are also described. The whole analysis was carried out in the MATLAB software package R2018a.

A. EXPERIMENTAL DATA DESCRIPTION

EEG data used in this work were collected from 30 neonates born at term equivalent age (38-42 weeks of gestation) with HIE treated with hypothermia at University Hospital Southampton (UHS) between February 2017 and August 2017. The infants were followed up under the clinical follow-up program at the UHS, with a neurological examination at age 24 months by a pediatric neurologist. Out of the 30 infants, 26 infants reached two years of corrected age and completed the follow-up assessment. A diagnosis of CP was made according to the criteria of the Surveillance of CP in Europe Working Group [26]. In this study, 20 infants had normal neurology, while six developed CP at 24 months of age. The EEGs were recorded from the infants on the neonatal intensive care unit within the first seven days after birth, during a period of restfulness with eyes closed for at least 20 minutes. Nineteen surface electrodes (C3, C4, CZ, F3, F4, F7, F8, FZ, FP1, FP2, O1, O2, P3, P4, PZ, T3, T4, T5 and T6) applied according to the international 10-20 system were used. Recordings were done by either a Nihon Kohden (sampling frequency 512 Hz, high-pass filter 0.08 Hz, the low-pass filter 300 Hz) or XLTEK (sampling frequency 512 Hz, high-pass filter 0.1 Hz, the low-pass filter 400 Hz) clinical video-EEG system. A consultant neurophysiologist examined all of the recorded EEGs and extracted a continuous clip with minimal artifacts (the average length of the clips is approximately two minutes). Secondary analysis of anonymized, routinely collected clinical data was approved by the HRA and Health and Care Research Wales, HCRW (Reference ID 20/HRA/0260; IRAS project ID 278072 University Hospital Southampton R&D protocol number RHM CHI1047).

B. DATA PREPROCESSING

The continuous resting-state data was pre-processed using EEGLAB, an open-source toolbox in MATLAB, to remove the remaining artifacts such as eye movement, muscle, heart activities, line noise, and signal discontinuity. The block diagram of the pre-processing steps is depicted in Fig. 2.

The data were initially filtered through a bandpass filter with the cut-off frequencies of 0.5 Hz and 45 Hz. Then, the bad channels were identified to make the data amenable for the analysis. EEGLAB automatically picks the bad channels based on two criteria: first, the flat channels, and second, the channels with large amount of noise determined based on their standard deviation. Subsequently, the bad channels (which were 7) were removed from each subject and not included in further analysis in any subject in our dataset. The remaining 12 channels were: C3, F3, F7, Fz, O1, O2, P3, P4, T3, T4, T5, and T6.

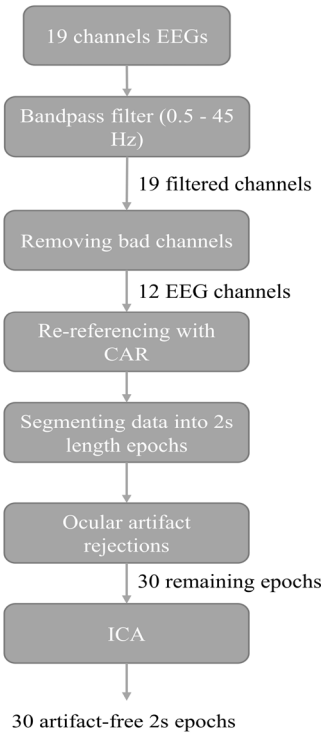

FIGURE 2. Block diagram of the pre-processing steps.

The data were then re-referenced by a common averaged reference (CAR) to reduce the confounding effects of the reference. After that, the continuous EEG was segmented into epochs of 2s length according to the typical approaches followed for EEG resting-state analysis [19]. Because EEG is a non-stationary signal in its nature and quasi-stationary only within short intervals, a 2s epoch is considered an appropriate length of time to capture the essence of its properties [27].

Ocular artifact, particularly eye movement, was automatically detected through the EEGLAB toolbox by setting the threshold value equal to 55 μV because such artifacts were defined as greater than this value [28]. Thus, each epoch containing values above this threshold was marked as a bad epoch. After this step, the remaining epochs were visually inspected to determine whether they were contaminated by high frequency, line noise, or discontinuity. The corrupted epochs were rejected and excluded from further analysis.

Independent component analysis (ICA) was then applied, using the runICA algorithm implemented in EEGLAB, to remove the remaining artefacts from the signals, such as muscle artefacts and cardiac activity. Thus, the EEG signals from the 12 channels are separated into their 12 constituent independent components (ICs), as the general rule of ICA is to find the N independent components from the N linearly mixed-signal (input channel data). These ICs are then projected back to the EEGs using the estimated separating matrix after the artefact-related ICs are manually eliminated [17].

Finally, a total of 12 channels, each with 30 artifact-free of 2s epochs per subject, were used in the next stage of the analysis.

C. N-A MULTIVARIATE EMPIRICAL MODE DECOMPOSITION

Empirical mode decomposition (EMD) [29], more specifically its noise-assisted multivariate extension (NA-MEMD) [30], was employed in this study to decompose the EEG signals into finite oscillation scales at the time domain. Multivariate mode decomposition (MEMD) was initially proposed by Rehman *et al.* [31] to solve the mode-alignment problem, which leads to a non-identical number of IMFs when analyzing a multivariate signal using the standard EMD. Later, Rehman *et al.* improved their method by proposing the NA-MEMD, which solves the mode-mixing –the second problem associated with the EMD. Mode-mixing arises when a single IMF contains different frequency ranges. NA-MEMD solves this issue by adding a multivariate independent white noise to the original multivariate signal, and then it processes the resulting composite using the MEMD algorithm.

Unlike other traditional decomposing methods such as band-pass filters, Short-time Fourier [32] and Wavelet transform [33], EMD-based methods do not require a predefined basis of the signal, and they decompose the time-series adaptively, through the Sifting process, from high to low-frequency components known as intrinsic mode functions (IMFs). The resulted IMFs should sum to a composite nearly identical to the original signal given by

$$x(t) = \sum_{i=1}^{n} IMF_i(t) + R_n(t) \tag{1}$$

where $x(t)$ is the original signal, t is the time, i is the IMF index, n is the total number of IMFs, and $R_n(t)$ is the residue of the signal $x(t)$ after n number of IMFs are extracted.

The procedure of the Sifting process of the NA-MEMD method starts by considering a sequence of n-dimensional vectors $\{v(t)\}_{t=1}^{T} = \{v_1(t), v_2(t), v_3(t), \ldots, v_n(t)\}$ that represents a multivariate signal with n components (including the original signals and the added noise), and a set of direction vectors $X^{Q_k} = \{x_1^k, x_2^k, x_3^k, \ldots\ldots, x_n^k\}$ along the directions given by angles $Q^k = \{Q_1^k, Q_2^k, \ldots, Q_{(n-1)}^k\}$ on an $(n-1)$-sphere. Then, the MEMD algorithm is applied according to the following steps:

1. Choose a suitable set of points for sampling on a (n-1) sphere.
2. Calculate a projection, denoted by $\{P^{Q_k}(t)\}_{t=1}^{T}$, of the input signal $\{v(t)\}_{t=1}^{T}$ along the direction vector X^{Q_k}, for all k (the whole set of direction vectors), giving $\{P^{Q_k}(t)\}_{k=1}^{K}$ as the set of projections.
3. Find the time instants $t_j^{Q_k}$ corresponding to the maxima of the set of projected signals $\{P^{Q_k}(t)\}_{k=1}^{K}$.
4. Interpolate $[t_j^{Q_k}, v\left(t_j^{Q_k}\right)]$ to obtain the multivariate envelope curves $\{e^{Q_k}(t)\}_{k=1}^{K}$.
5. For a set of K direction vectors, the mean $m(t)$ of the envelope curves is calculated as $m(t) = \frac{1}{K}\sum_{k=1}^{K} e^{Q_k}(t)$.
6. Extract the detail $IMF_i(t)$ using $IMF_i(t) = v(t) - m(t)$. If the detail $IMF_i(t)$ satisfies the IMF conditions [29],

apply the above procedure to $v(t) - IMF_i(t)$, otherwise apply it to $IMF_i(t)$.

The Sifting process ends when the detail is monotonic, and no more IMFs can be extracted from it. It is important to note that the added noise is never mixed with the original data, as it resides in a different subspace which is discarded at the end of the Sifting process.

D. COMPLEXITY ANALYSIS

A growing body of literature has reported atypical EEG complexity associated with different brain disorders [24]. The interpretation of the complexity changes differs according to the physiological parameters and the clinical or neurodevelopmental condition studied. Nevertheless, there is increasing evidence that various pathological processes are associated with abnormal and often (but not always) reduced measures of physiological complexity [34]. Complexity analysis is utilized to provide a nonlinear estimation of the dynamical brain activity. The entropy-based features are commonly used to quantify the complexity of a time series [24]. A brief description of the entropies employed in this study is given in the following.

1) SAMPLE ENTROPY

SampEn was developed by Richman and Moorman [35] to estimate the randomness or irregularity of a time series. It is a modification of approximate entropy (ApEn) [36], improving its sensitivity to the signal length and immunity to the noise in the data [35]. Both measures have been widely used for the analysis of physiological datasets. SampEn is the probability that two similar patterns for m point remain similar at the next $m+1$ point within a tolerance r. Thus, for the time series $x(i)$ of length N, SampEn is given by:

$$SampEn(m, r, N) = -\ln[A^m(r) / B^m(r)], \tag{2}$$

where

$$A^m(r) = (N-m)^{-1} \sum_{i=1}^{N-m} C_i^{m+1}(r), \tag{3}$$

$$B^m(r) = (N-m)^{-1} \sum_{i=1}^{N-m} C_i^{m}(r), \tag{4}$$

$$C_i^m(r) = (N-m-1)^{-1} C_i, \quad i = 1, 2, \ldots, N-m, \tag{5}$$

where m is the embedding dimension, $B^m(r)$ is the likelihood that $X_m(i)$ and $X_m(j)$ is matching for m points, while $A^m(r)$ is the likelihood that $X_m(i)$ and $X_m(j)$ will match for $m+1$ points. $C_i^m(r)$ is the probability of a vector $X_m(i)$ being similar to $X_m(j)$ within a tolerance r, C_i is the number that the distance between the two vectors $X(i)$ and $X(j)$ is smaller than r, and a vector $X_m(i)$ $(1 \le i \le N-m+1)$ reconstituted of this series, and is given by: $X_m(i) = \{X(i), X(i+1), \ldots, X(i+m-1)\}$.

A small value of SampEn indicates similar patterns and, therefore, a low complex time series, while a large value reflects a time series with high complexity.

For optimal estimation of SampEn, previous studies have recommended the embedding dimension $m = 2$ or 3, and the tolerance $r = 0.1$ - 0.25 of the standard deviation of the signal [37], [38]. In this exploration, we checked different parameter settings in these recommended ranges to check the robustness of the estimated SampEn measures against the small changes in parameters.

2) PERMUTATION ENTROPY

Bandt and Pompe proposed PEn to measure the irregularity of the signal by quantifying the occurrence of ordinal patterns within the time series [39]. Characterized by its simplicity and robustness, PEn measures the signal's irregularity by comparing the neighboring values of multidimensional ordinal sequence vectors, which are formed based on embedding dimension and time delay parameters. For the time series $x(i)$ of length N that reconstructed using the embedding dimension m, the normalized PEn is given by:

$$PEn = -\sum_{i=1}^{K} p_i \log p_i \tag{6}$$

where K is the number of different permutation equal to $N-m+1$, and p_i is the probability of the *ith* permutation. The smaller the value of PEn, the less complex the time series is [39].

PEn estimation depends on the selected values of embedding dimension m and time delay L used to reconstruct the sequence vectors. The appropriate selection of these parameters is necessary for proper PEn estimation. Olofsen *et al.* [40] suggested the values of $m = 3$ and $L =$ 1-2 for this purpose. This study calculated the PEn using these recommended values to investigate whether the small changes in the embedding parameters could affect the entropy estimation.

3) SPECTRAL ENTROPY

SpEn is a standard EEG complexity measure that computes the randomness of the signal spectrum. Thus, unlike SampEn and PEn, SpEn estimates the signal irregularity in the frequency domain. For this end, SpEn applies the Shannon entropy concept to the normalized power spectral density (PSD) of the signal such that,

$$SpEn = -\sum_{i=1}^{N} p_i \log p_i, \tag{7}$$

where p_i is the probability of PSD at each frequency point i, and N is the total frequency points. The sum of all p_i is equal to 1 [41]. SpEn is an efficient way to reflect the degree of skewness in the frequency distribution. A high value of SpEn indicates a flat, uniform spectrum with a broad spectral content, and a low value of SpEn describes a spectrum with all the power condensed into a single frequency point [42].

E. WPLI-BASED FUNCTIONAL BRAIN CONNECTIVETY ABNALYSIS

Functional brain connectivity measures the interdependency among activities of distinct and distant brain regions by using statistical methods, such as correlation, covariance, and phase synchronization (PS) [43]. PS is a nonlinear method used to measure the phase relations of electrophysiological brain signals [43]. Such a method could reveal the underlying

information exchange and relationship strength between each pair of the signal's sources. Thus, PS has been chosen to compare the functional brain connectivity of the infants who developed CP and the normal group.

WPLI is a phase-based functional connectivity method that was used, in this study, for the quantification of PS. It was proposed to settle the well-known problem of phase-lag index (PLI), alleviating the sensitivity to noise that might exist in case of small perturbation of phase, which could turn phase lags into leads and vice versa and cause discontinuity of the measure [44]. To reduce this issue, WPLI gives an improved estimation of connectivity by weighting the phase difference according to their magnitudes of the imaginary component of the cross-spectrum. In this way, the phase differences, which are at the high potential of changing their true sign with small noise perturbations, are weighed by a small value of the imaginary component. Consequently, they have a lower influence on estimating connectivity.

Mathematically, WPLI can be defined as:

$$WPLI = \frac{|\langle|\Im(X)|\text{sign}\,(\Im(X))\rangle|}{\langle|\Im(X)|\rangle} \tag{8}$$

where $\Im(X)$ is the imaginary component of the cross-spectrum X. The WPLI value is either one, denoting to the presence of synchronization, or zero, refereeing to no synchronization between two signal sources.

WPLI quantifies the strength of phase coupling between neural oscillators by estimating the instantaneous phase from the time-series signal. It is important to derive the WPLI from narrow-band components in each source to get the phase's intending physical interpretation. For that reason, herein, the NA-MEMD method was applied to decompose EEG signals into the intrinsic components before calculating the WPLI matrix.

F. GRAPH THEORY ANALYSIS

In the graph theory analysis, the brain is represented as a network where the nodes correspond to distinct brain regions (or EEG electrodes in EEG-based functional brain connectivity derivation) and the edges representing the functional connections between them identified by the WPLI index. Traditionally, the graph network is characterized over two-level scales: nodal and global. The nodal property gives us insight into the node's property in terms of its connectivity with the neighboring nodes.

In contrast, the global metrics reveal the information flow of the whole network as well as any specialized local processing. In this study, we mainly investigated the global properties of the network owing to the neuroimaging results, which suggested hyper-connection and hypo-connection alteration associated with the brain function of individuals with CP [16]. These two properties could be captured by the global network metrics: transitivity, global efficiency, radius, diameter, characteristic path length, and clustering coefficient. Thus, these six graph parameters were chosen to be used in this study as they could provide great insight into the information flow in the brain of infants diagnosed later with CP. These features were calculated using the brain connectivity toolbox (BCT) [45] in a MATLAB environment, and a brief description of them has been shown in Table 1.

TABLE 1. List of the graph parameters that used for characterizing a network.

Feature	Description
Transitivity (TRS)	Reflecting connectivity of given region to its neighbors. The network with high transitivity implies it contains groups of regions that are densely connected internally.
Global efficiency (GE)	Representing the inverse of the distance between the regions. It measures the network efficiency in terms of how well the brain network integrated and how easily the information transfer between distinct brain regions.
Radius (RDS)	Measuring the shape of the network and it is the minimum of the network eccentricity. Eccentricity assesses the integration ability of the network; high eccentricity refers to a more integrated network.
Diameter (DMT)	Measuring the shape of the network and it is the maximum of network eccentricity.
Characteristic path length (CPL)	Representing the average distance between all pairs of brain regions in the network. It indicates how easily information transforms across the network.
Clustering coefficient (CC)	Measuring the extent of local interconnectivity within the network by calculating the mean of the clustering coefficients at each region in the network where the clustering coefficient of a region is defined as the number of existing connections among the region's neighbors divided by all their possible connections [46]. A brain network with a high clustering coefficient refers to more locally efficient network.

G. NA-MEMD-BASED FEATURE EXTRACTION PROCESS

The NA-MEMD method was utilized to decompose the EEG signals before extracting the two fundamentally feature classes, namely entropies and graph-theoretic measures. To characterize the multi-subject neural recordings collected over multi-channel and multi-epochs, our proposed NA-MEMD-based analysis consists of the following steps:

1. For each channel, the data points from all infants were combined to obtain a multivariate signal. Combining signals from different sources and constructing a multivariate signal for NA-MEMD analysis to acquire aligned IMFs has been employed in the literature [47]. Hence, we constructed twelve different matrices (i.e., one matrix for

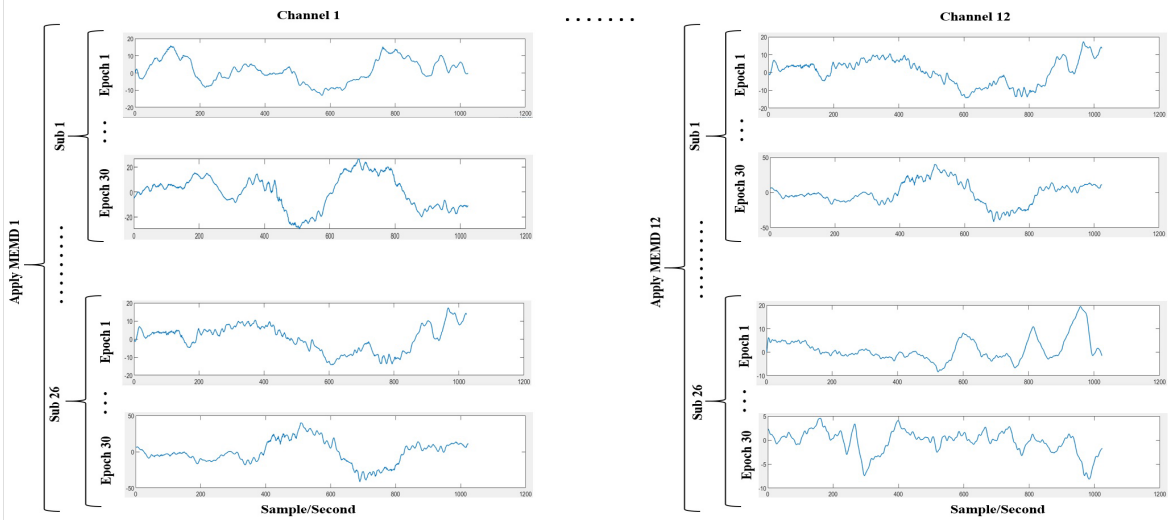

FIGURE 3. The proposed simultaneous decomposition method of the EEG signals.

each channel); each of them has the dimensionality of $N_s \times N_t \times N_e$, where N_s denotes the number of subjects (which is 26), N_t indicates the number of temporal samples (which is 1024), and N_e is the number of epochs of each subject (which is 30).

2. Each of the twelve matrices was reshaped into a two-dimensional time series of the dimension $[N_s \times N_e] \times N_t$ before decomposing it by the NA-MEMD algorithm. Following this step, we ensure that all IMFs are aligned not only across infants but also across epochs. A similar process has been adopted previously by [48]. Fig. 3 illustrates the decomposition process.
3. After the decomposition, different numbers of IMFs were produced from different electrodes. The EEG channels that yielded the lowest number of IMFs upon the decomposition gave ten modes. Thus, to unify the number of IMFs among channels, the first ten IMFs of each channel were considered. Fig. 4 shows the extracted IMFs of a sample epoch from a channel that gave ten IMFs.
4. The frequencies of each IMF were then acquired by the fast Fourier transform (FFT). After inspecting the power spectra of IMFs, IMF1 and IMF2 were considered noisy as they contained different oscillatory components. Thus, these modes were excluded from further analysis. IMF10 was also ignored as it represented the residue mode of some EEG channels, which might give unreal information about the signal. The scales of the remaining IMFs were localized approximately around the following ranges: IMF3 (30-35 Hz), IMF4 (20-25 Hz), IMF5 (10-13 Hz), IMF6 (5-8 Hz), IMF7 (3-4 Hz), IMF8 (2-3 Hz), and IMF9 (0.5-2 Hz). Referring to the five traditional brain waves [17], IMF3 to IMF6 frequencies belong to the gamma, beta, alpha and theta bands, respectively, while IMF7, IMF8 and IMF9 all belong to the delta brain wave.

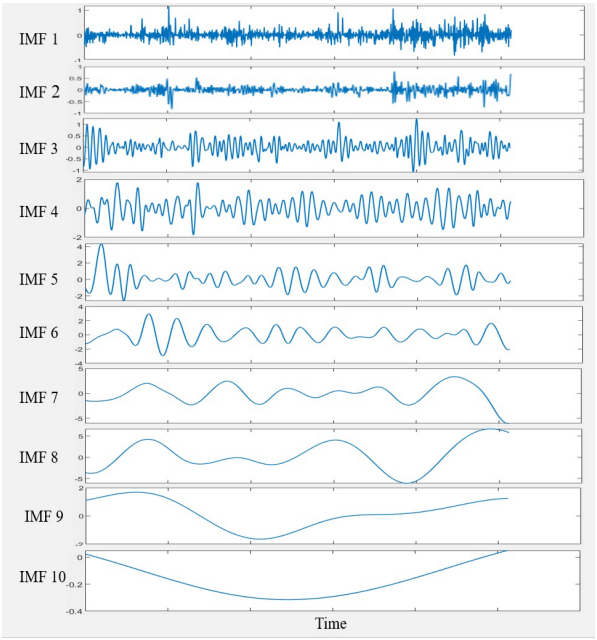

FIGURE 4. An example of a set of IMFs resulting from the NA-MEMD method.

5. After IMF selection, we ended up with a dataset of the following dimensionality for each subject: $N_c \times N_i \times N_e \times N_t$, where N_c is the number of channels which is 12, N_i is the selected number of IMFs, which is 7 (IMF3 – IMF9), N_e is the number of epochs which is 30, and N_t is the number of the samples which is 1024.
6. For each channel and each IMF, the proposed entropy measures were computed for each epoch. The calculated features were then averaged among the epochs to obtain one SampEn, one PEn, and one SpEn for each IMF signal. Thus, for each subject and each IMF signal, we ended up

with 36 features (3 features × 12 channels). These features were then used to train and test the RUSBoost classifier.

7. Before calculating the WPLI-based features, the alignment of the selected IMFs (IMF3 – IMF9) among channels was investigated and confirmed.
8. For each IMF and each epoch, the WPLI connectivity matrix was computed between the twelve channels. The generated WPLI matrices were then averaged over the epochs to get one connectivity matrix for each IMF signal.
9. Each connectivity matrix was then transformed into a connectivity network, and the graph-theoretic parameters were calculated to quantify its properties. Thus, for each subject and each IMF signal, we ended up with six graph-theoretic features. These features were then used to train and test the RUSBoost classifier.

H. STATISTICAL ANALYSIS

Kruskal-Wallis test [49] was adopted in this study to verify whether the discriminatory capability of the selected set of features (entropies and the graph-theoretic features in the NA-MEMD domain) was statistically significant between the two classes (infants who developed CP and those who did not). The test was carried out using the MATLAB statistics toolbox.

In general, the difference between groups is statistically significant when the p-value falls below a threshold known as the level of significance (α), usually equal to 0.05. However, a proper adjustment is required if several independent tests are simultaneously conducted (known as multiple comparisons). Thus, Benjamini–Hochberg false discovery rate [50], a well-known approach for such adjustment, was employed in this study.

For complexity analysis, the Kruskal-Wallis test was utilized to determine the capability of the three entropy features computed from each IMF (21 p-values: 3 features × 7 scales). Benjamini–Hochberg correction was employed to control these multiple comparisons, and the value of α has been corrected from 0.05 to 0.0019.

For WPLI, the Kruskal-Wallis test was also used to assess the discriminant capabilities of the six graph-theoretic features computed from each IMF (42 p-values: 6 features × 7 scales). Utilizing Benjamini–Hochberg correction, the p-value was corrected to 0.02.

I. FEATURE SELECTION

The proposed complexity analysis method employed 36 features for each subject extracted from each IMF signal (3 entropies × 12 channels). This situation may lead to the overfitting problem as the number of features are greater than the number of training samples (the 26 subjects). Selecting the highly informative features from a larger pool of available ones is recommended to optimize the classification performance [51].

Different feature selection techniques have been proposed in the literature [51]. Due to its simplicity and reliability [51], we employed the scalar feature selection method according to the following procedure:

1. Normalize the features to zero mean and unit variance to remove the bias from features having high values.

$$\hat{x}_i = \frac{x_i - \bar{x}}{\sigma}, \quad i = 1, 2, \ldots, N \tag{9}$$

where $\hat{x}_i$ is the normalized value, N be the number of features, x_i is the feature i, $\bar{x}$ the mean and σ be the standard deviation.

2. Rank the features in descending order according to the Fisher's discriminant ratio (FDR) measure.

$$FDR = \frac{(\mu_1 - \mu_2)^2}{(\sigma_1^2 + \sigma_2^2)} \tag{10}$$

where μ_1 is the mean of the first class, μ_2 is the mean of the second class, σ_1^2 and σ_2^2 are the variance of the first and second class, respectively.

3. Compute the cross-correlations among the top-ranked feature (with the index i_1) and each remaining features. The index, i_2, of the second most important feature is computed as

$$i_2 = \arg\max \{a_1 C_j - a_2 \left|\rho_{i_1,j}\right|\}, \quad j \neq i_1 \tag{11}$$

which incorporates the feature ranking value C for the jth feature, and the cross-correlation ($\rho_{i_1,j}$) between the best feature (i_1) and feature $j \neq i_1$. The parameters a_1, a_2 are weighting factors.

4. The rest of the features are ranked according to

$$i_k = arg\ max\{a_1 C_j - \frac{a_2}{k-1} \sum_{r=1}^{k-1} \left|\rho_{i_r,j}\right|\}, \quad j \neq i_r \tag{12}$$

for $r = 1, 2, \ldots, k-1$, and $k = 3, 4, \ldots, m$.

The top-ranked features were then selected to train and test the RUSBoost classifier.

J. CLASSIFICATION ALGORITHM

The choice of our classifier was guided by the class imbalance in our sample set, as described in section A – 20 neonates with the normal neuromotor outcome and six with CP. Therefore, a RUSBoost classifier was adopted to discriminate between the two groups as it is efficient in alleviating the problem of class imbalance. RUSBoost is a hybrid method combining random undersampling with a boosting approach. A random undersampling algorithm works by randomly removing instances from the majority class until the intended balance is achieved [52]. Boosting is an ensemble method that constructs a robust classifier from several weak classifiers (such as a decision tree) by building a model from training data and then formulating a second model that seeks to correct the existing error in the previous models. This process is repeated until the training set is predicted correctly [52]. RUSBoost has several advantages, such as computational simplicity, reliability and short training time, making it a useful solution for learning from imbalanced data. The classifier training

was performed using Classification Learner App within the Statistics and Machine Learning Toolbox in MATLAB.

Data overfitting is one of the most common problems that affect classification performance in which the model performs well on training data but poorly fits new ones. Overfitting risk increases for several reasons, such as an imbalanced or limited number of samples and a large number of features. In this study, while the RUSBoost classifier was employed to reduce the effect of imbalanced data, cross-validation was used to mitigate the limited number of samples problem. Particularly, the leave-one subject-out cross-validation (LOSOCV) method was employed, as it is useful when the same data need to be used for both training and testing (due to the limited data samples) [53]. Given N subjects (herein $N = 26$), LOSOCV uses the feature vectors of $N-1$ subjects for training and the vector of the remaining subject for testing. This procedure is repeated N times, leaving out the data of a different subject each time. Finally, the classifier performance is obtained by averaging the N independent results. Thus, the same dataset is utilized for training and testing, and, at the same time, the testing is carried out on samples that have not been seen in the training [53].

The performance of the classifier was evaluated using the conventional measures of accuracy (ACC), sensitivity (SNS), specificity (SPC), and area under curve (AUC).

III. RESULTS

This section illustrates the details and outcomes of employing the two proposed set of features and presents the significance of the results.

A. ENTROPY ANALYSIS RESULTS

Fig. 5 presents the results of the Kruskal-Wallis test for SampEn, PEn, and SpEn, respectively, when computed from each IMF for all electrodes to discriminate between the CP and normal groups. Different embedding dimensions m and tolerances r were explored for SampEn estimation as suggested by [37], [38]. The PEn was also calculated using time delay $L = 1$ and $L = 2$, and embedding dimension $m = 3$ as recommended by Olofsen *et al.* [40].

It can be noticed from the figure that the lowest p-values were obtained when all entropy features were calculated from IMF5, indicating good discriminatory capability between the infants with CP and infants with normal neurology. The figure also shows the robustness of SampEn and PEn measures with the small changes of the embedding parameters. The p-values of SampEn, PEn, and SpEn estimated from IMF5 were all significant and equal to 0.0019, 0.0013, and 0.0004, respectively.

To explore how the entropies calculated from IMF5 differ between infants with CP and infants with normal neurology, the distributions of complexity measures of both groups have been estimated as presented in Fig. 6. Compared to the normal group, the CP group showed lower entropy values, indicating

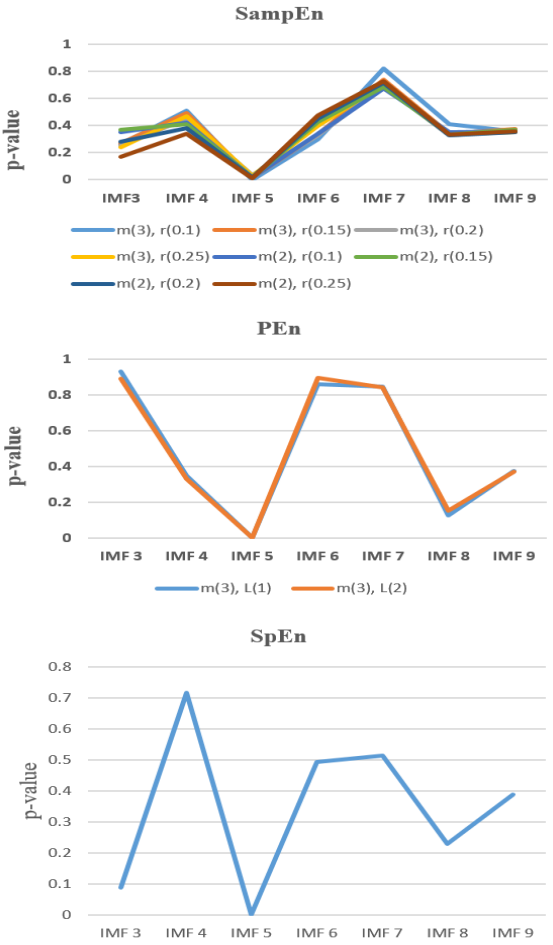

FIGURE 5. P-values of the entropy features comparing CP and normal groups for each IMF.

a complexity reduction, specifically in the alpha band–the frequency band corresponding to IMF5. Due to their significant discriminant capability between the CP and normal groups, entropies features of all electrodes computed from IMF5 were selected to train the RUSBoost classifier.

To prevent overfitting, the classifier was trained on different subsets of the feature vector. For each subset, the features were selected using the scalar feature selection method described previously. In practice, classification results of different numbers of selected features could be explored, and the one that results in the best performance might be considered [51]. Thus, we started by investigating the performance of the top 20 high-ranked features, where the role of thumb is not to exceed the number of the training samples (which is 26) [51]. The top 15, top 10, top 5, top 3, top 2, and top 1 features were also investigated. Table 2 gives the LOSOCV results when the classifier was trained and tested on the entire feature set and the top selected ones. It can be inferred that the classifier's performance was generally enhanced by reducing the number of features. The best classification results were achieved using the top 5 selected features.

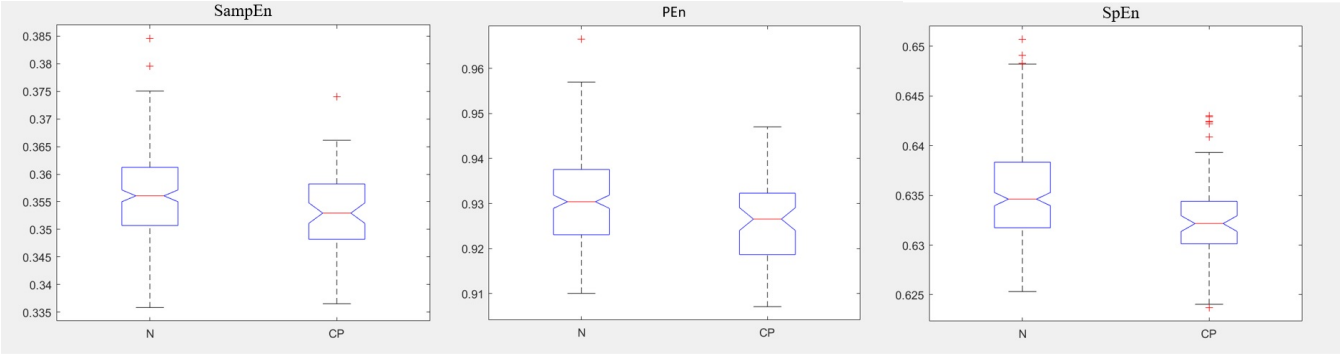

FIGURE 6. Box plots of the distribution of the complexity measures extracted from IMF5 signals of infants with CP and infants with normal neurology. The entropy values of CP show lower values compared to the normal subjects.

TABLE 2. Performance of the RUSBoost classifier using different groups of complexity features.

Entropy Features	ACC	SNS	SPC	AUC
All 36 features	69.2%	67%	70%	0.71
Top 20	73.1%	67%	75%	0.65
Top 15	73.1%	67%	75%	0.75
Top 10	76.9%	83%	75%	0.79
Top 5	84.6%	83%	85%	0.87
Top 3	80.8%	80%	83%	0.82
Top 2	76.9%	80%	67%	0.73
Top 1	76.9%	80%	67%	0.77

TABLE 3. p-values of the graph-theoretic features. Graph feature that is statistically significant is indicated in boldface.

	TRS	GF	RDS	DMT	CPL	CC
IMF3	0.3942	0.4289	0.5032	0.3009	0.3942	0.3942
IMF4	0.9515	0.9515	0.5032	0.3302	0.9031	0.9515
IMF5	0.6264	0.5428	0.6701	**0.0207**	0.8077	0.6316
IMF6	0.4652	0.4652	0.7609	0.2476	0.6701	0.6679
IMF 7	0.2476	0.3009	0.715	0.9515	0.3613	0.2476
IMF8	0.5839	0.5839	1	0.3942	0.6164	0.5839
IMF9	0.2235	0.2476	0.2476	0.3613	0.2476	0.6864

B. WPLI-BASED FUNCTIONAL BRAIN CONNECTIVITY RESULTS

Table 3 summarizes the results of the Kruskal-Wallis test for the graph-theoretic features. The features with lower p-values are shown with boldface in the table, indicating a statistically significant difference.

The results demonstrate that the difference between the two populations is particularly distinct using the diameter feature computed from IMF5. The boxplot presented in Fig. 7 indicates that the diameter of the CP group was significantly higher than the normal one.

The diameter feature estimated from IMF5 was selected to be used in the classification stage due to its significant discriminability between the study groups. The performance of the RUSBoost classifier was evaluated using LOSOCV, and a good result of 80.8% ACC, 67% SNS, 85% SPC and 0.79 AUC was also achieved.

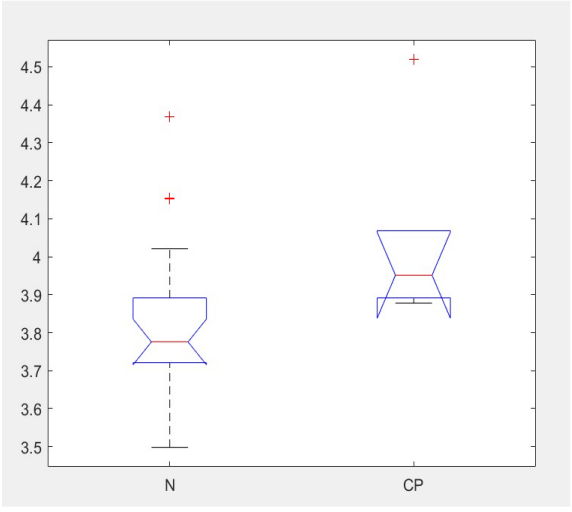

FIGURE 7. Box plot of the distribution of the diameter feature extracted from the IMF5 component of infants with CP and those with normal neurology. The diameter values of infants with CP are higher than those of normal subjects.

IV. DISCUSSION

This study carried out a qEEG analysis in a machine learning framework to identify clinical biomarkers that could distinguish between term-born infants with neonatal HIE, who developed CP by the age of two, and those with normal neuromotor development. Early identification of those at the highest risk of adverse outcomes enables targeted early interventions and provides families with psychological and financial support.

Both complexity and functional connectivity characteristics of the resting EEG signals were explored to provide a multivariate investigation of the abnormal brain function of infants with CP. To the best of the authors' knowledge, this is the first study employing such qEEG measures, particularly nonlinear entropies and graph-theoretic features of WPLI in the NA-MEMD domain, to explore brain dynamics of children with neonatal HIE who developed CP.

The main challenge of this study was the limited and imbalanced number of samples in the dataset, as out of the 26 infants under prospective monitoring, only 6 developed CP at 24 months. Because this is a common problem in clinical studies, the machine learning community devoted a significant effort to establishing classification techniques for such limitations. LOSOCV was employed to reduce the effect of the limited number of samples, while the RUSBoost classifier was used to handle the imbalanced classes issue.

Entropy measures were the first class of features investigated to differentiate between the infants with CP and infants with normal neurology. While most of the well-known entropy measures quantify the regularity of a time series represented on a single scale [24], Multiscale entropy [54], for example, measures the complexity considering different scales inherent in the signal. Though powerful, the multiscale entropy method is not well adapted for studying the nonlinear and non-stationary signals due to its linear extraction of scale [55]. Subband wavelet entropy (SWE) [56] was also proposed to measure Shannon entropy from multiscale components. However, SWE is based on the wavelet method, which relies on predefined frequency ranges for the decomposition process. In the present work, we addressed these issues by computing the proposed entropies over different signal scales/IMFs extracted by NA-MEMD, which decomposes the signals adaptively and considering the nonlinear and non-stationary nature of EEGs [57], [48].

The statistical analysis results showed that the best discriminatory capability of the three entropies (SampEn, PEn, and SpEn) was when they were extracted from IMF5 - the component corresponds to the alpha brain wave [17]. These results were robust with the small changes in the entropy estimation parameters. Particularly, the infants with CP exhibited significantly lower entropies at the alpha-band compared to the normal group. This finding suggests that brain function is impaired in infants who developed CP, leading to lower complexity in their EEG signal.

Gao *et al.* [15] also found a deficit in the complexity of alpha-band signals of individuals with CP. However, they reported a higher global complexity in their signals compared to the controls. This inconsistency might be due to the differences in the complexity measures between the two studies. While we employed nonlinear complexity to measure the temporal regularity of the signals, they used the linear omega complexity to assess the degree of synchronization between spatially distributed brain areas. Furthermore, the age at investigation was different from our study. Gao *et al.* exploration was performed on male adolescent patients while we investigated newborns' brain complexity. Sajedi *et al.* [22] also reported a higher EEG complexity in children with CP employing the fractal dimension as a nonlinear measure of time series regularity. Nevertheless, they computed the complexity for the broad-band signals (1-30Hz) and didn't consider the complexity of each brain wave independently. In addition, they reported the enhanced complexity for the interior brain area, while we computed the complexity for all regions.

WPLI-based functional brain connectivity measure was the second set of features explored in this study. Although the coherence, phase-locking value (PLV) and PLI are the most popular methods for quantifying functional brain connectivity, they are associated with several shortcomings that WPLI could overcome. Coherence is a linear approach affected by volume conduction. The PLV and PLI are both advantaged by being nonlinear methods. However, PLV is also affected by volume conduction, while PLI is associated with the discontinuity problem. As discussed earlier in the methodology section, WPLI improved PLI by weighting the phase lags according to their magnitudes of the imaginary component of coherence (ImCoh). Even though WPLI uses a minor quantity of coherence, it has been proven that ImCoh can diminish the volume conduction effects, i.e., only the real coherence part related quantities are that affected by the conduction problem.

In line with complexity results, the best discrimination capability of the graph-theoretic measures was achieved using the alpha-band component of the signals. Particularly, the statistical results show an increase in the diameter feature estimated from IMF5 of the infants with CP compared to the controls. This result implies the global hypoconnectivity, indicating that the CP's brain network is less integrated, and accordingly, the information transfer across the network is less efficient. This finding is consistent with the previous studies that found the hypoconnectivity between the right and left hemispheres in individuals with CP using the coherence-based measures [18]–[20]. On the other hand, different studies have reported the disruption of brain connectivity revealed at the alpha band in individuals with CP [16]–[20].

Due to their significant results, entropies and graph-theoretic features (basically the diameter) calculated from IMF5 were used to train and test the RUSBoost classifier. Comparable classification results have been achieved using the two classes of features; The classifier performance using the entropy features reached 84.6% ACC, 83% SNS, 85% SPC, and 0.87 AUC, along with 80.8% ACC, 67% SNS, 85% SPC, and 0.79 AUC using the diameter feature.

The methodology and findings of our investigation have been compared to the state-of-the-art research, which used qEEG analysis to characterize CP brain abnormalities. The pros and cons of the methodologies followed by the existing techniques have been discussed earlier in the introduction section. Table 4 summarizes the methods as well as the findings of previous research and the current study.

It could be inferred from the table that a deficit in the alpha band was reported by almost all research. Machine learning frameworks have been employed in only two explorations [18], [22], which reached 91.7% ACC, 100% SNS, 83.3% SPC and 94.8% ACC, 92.5% SNS, 97.2% SPC, respectively. These results are slightly better than the classification performance of our proposed method (84.6% ACC, 83% SNS, 85% SPC). However, the measures employed

TABLE 4. Comparison of the qEEG state-of-the-art methods employed for CP classification.

Authors	Dataset	Features	Decomposition method	Evaluation method	findings
Gao *et al.* [15]	Adolescent 14-22 years, CP (n=15) and N (n=15)	**Microstate** to measure temporal correlation. **Omega complexity** to assess spatial correlation.	FFT	Statistical analysis	**Microstate:** Higher temporal complexity in CPs compared to control. **Omega complexity:** Higher global omega complexity in CPs at the alpha band compared to control.
Gao *et al.* [16]		Detrended fluctuation analysis (DFA) to measure temporal correlation	FFT	Statistical analysis	The DFA exponents at alpha and beta bands were significantly attenuated in the CPs compared to controls.
Koeda and Takeshita [18]	Children 7-15 years, CP (n=12) and N (n=15)	PSD and coherence measures	FFT	Statistical analysis	**PSD:** No significant difference in PSD. **Coherence:** Lower interhemispheric coherence (ICoh) at the occipital region for alpha-band, higher ICoh at the frontal region for theta-band, and higher intrahemispheric coherence (Hcoh) at the left hemisphere for the delta, theta, and beta bands in the CPs compared to controls.
				Discriminant Analysis classifier	Performance of 91.7% ACC, 100% SNS, 83.3% SPC has been reached using the statistically significant features.
Kułak et al. [19]	Children 6-14 years, CP (n=12) and N (n=21)	PSD and coherence measures	FFT	Statistical analysis	**PSD:** Significant differences between the CP and control over the left and right hemispheres for the delta, theta, alpha and beta bands. **Coherence:** lower ICoh at the temporal, parietal and occipital regions for the alpha band, lower ICoh at the frontal, central, parietal and occipital regions for the beta band, higher ICoh at the frontal and temporal regions for the theta and delta bands and higher HCoh at right hemisphere for the alpha band in individuals with CP compared to control.
Kulak and Sobaniec [20]	Children 6-15 years, CP (n=26) and N (n=28)	PSD and coherence measures	FFT	Statistical analysis	**PSD:** Significant differences between the CP and control over the left and right hemispheres for the delta, theta, alpha and beta bands. **Coherence:** lower ICoh at the temporal, parietal and occipital regions for the alpha band in the CPs compared to controls,
Sajedi et al. [22]	Children 4-14 years, CP (n=26) and N (n=26)	PSD and fractal dimension to measure temporal complexity.	Welsh's method	Statistical analysis	**PSD:** A higher delta and lower theta and alpha powers were found in CPs compared to controls. **Complexity:** A higher EEG complexity at the interior region for the range (1-30Hz) in CPs compared to controls.
				Enhanced probabilistic neural network (EPNN) classifier	Performance of 94.8% ACC, 92.5% SNS, 97.2% SPC have been reached using the statistically significant features.
Current study	Term HIE infants 1-7 days after birth, CP (n=6) and N (n=20)	SampEn, PEn and SpEn to measure temporal complexity, and Graph-theoretic features of WPLI to measure functional connectivity.	NA-MEMD	Statistical analysis	**Complexity:** A lower EEG complexity at the alpha band in CPs compared to controls. **Connectivity:** A global hypoconnectivity at the alpha band in CPs compared to controls.
				RUSBoost classifier	**Complexity:** Performance of 84.6% ACC, 83% SNS, 85% SPC, 0.87 AUC was reached using the complexity features. **Connectivity:** 80.8% ACC, 67% SNS, 85% SPC, 0.79 AUC was reached using the graph-theoretic features.

herein (WPLI and entropy measures in the NA-MEMD domain) can overcome the issue of the coherence, PSD and fractal dimension measures used in [18], [22].

We can generally argue that our exploration's novelty is represented by using qEEG measures to predict CP at infancy. Moreover, using WPLI and entropy measures can handle all limitations raised with other qEEG measures used in the literature, including the assumption of linearity and stationarity of the EEG signals and the volume conduction issue, mainly associated with the coherence measure.

Additionally, state-of-the-art studies often analyze the signals using time-frequency methods that rely on the predefined traditional brain waves. This scenario raises an issue where the ranges of neural oscillations of interest may vary among subjects, specifically between infants and older individuals [21]. This limitation has been settled in our proposed approach using the NA-MEMD method, which decomposes the time series adaptively. Hence, all potentially meaningful subject-specific brain dynamics inherent in the signals were included in the analysis.

In summary, our findings suggest that both complexity and connectivity features computed at the alpha band could discriminate well between infants who later develop CP and those with later normal neurology. These features could be used as biomarkers for a very early prediction of CP, which in turn enables the possibility of developing an appropriate intervention strategy to improve motor outcome. However, a much larger trial with a more significant population and a variety of perinatal and neonatal neurological complications needs to be conducted before this method could be considered for clinical application.

V. CONCLUSION

The proposed framework successfully discriminated resting-state EEGs of term-born infants with neonatal HIE who developed CP by the age of two years from those with the normal neuromotor outcome. Advanced complexity and functional connectivity measures in the NA-MEMD were assessed using statistical analysis and a machine learning framework. Both classes of features achieved good classification performance that reached 84.6% ACC, 83% SNS, 85% SPC and 0.87 AUC. Moreover, EEG complexity features (as indexed by SampEn, PEn, and SpEn) and graph-theoretic parameters (particularly diameter) of alpha-band may be considered biomarkers for early CP prediction.

Even though this study can be viewed as a promising attempt towards building an aiding tool for early prediction of CP, more work needs to be carried out in the future, with a larger and more balanced dataset and other classifiers.

ACKNOWLEDGMENT

Dalal Bakheet and Noura Alotaibi are awarded the scholarship from the Scholarship Program of the University of Jeddah, Jeddah, Saudi Arabia, for the Ph.D. study at the University of Southampton, Southampton, U.K.

REFERENCES

[1] B. Hagberg, G. Hagberg, and I. Olow, "The changing panorama of cerebral palsy in Sweden," *Acta Paediatrica*, vol. 73, no. 4, pp. 433–440, Jul. 1984.

[2] P. Rosenbaum, "The definition and classification of cerebral palsy: Are we any further ahead in 2006?" *NeoReviews*, vol. 7, no. 11, pp. e569–e574, Nov. 2006.

[3] U. Tonmukayakul, S. T. F. Shih, H. Bourke-Taylor, C. Imms, D. Reddihough, L. Cox, and R. Carter, "Systematic review of the economic impact of cerebral palsy," *Res. Develop. Disabilities*, vol. 80, pp. 93–101, Sep. 2018.

[4] M. Hadders-Algra, "Early diagnosis and early intervention in cerebral palsy," *Frontiers Neurol.*, vol. 5, pp. 1–13, Sep. 2014.

[5] H. van Laerhoven, T. R. de Haan, M. Offringa, B. Post, and J. H. van der Lee, "Prognostic tests in term neonates with hypoxic-ischemic encephalopathy: A systematic review," *Pediatrics*, vol. 131, no. 1, pp. 88–98, Jan. 2013.

[6] H. C. Glass, Y. Li, M. Gardner, A. J. Barkovich, I. Novak, C. E. McCulloch, and E. E. Rogers, "Early identification of cerebral palsy using neonatal MRI and general movements assessment in a cohort of high-risk term neonates," *Pediatric Neurol.*, vol. 118, pp. 20–25, May 2021.

[7] L. S. de Vries, I. C. van Haastert, M. J. N. L. Benders, and F. Groenendaal, "Myth: Cerebral palsy cannot be predicted by neonatal brain imaging," *Seminars Fetal Neonatal Med.*, vol. 16, no. 5, pp. 279–287, Oct. 2011.

[8] M. Bosanquet, L. Copeland, R. Ware, and R. Boyd, "A systematic review of tests to predict cerebral palsy in young children," *Develop. Med. Child Neurol.*, vol. 55, no. 5, pp. 418–426, May 2013.

[9] J. C. Harteman, F. Groenendaal, M. C. Toet, M. J. Benders, I. C. Van Haastert, R. A. Nievelstein, C. Koopman-Esseboom, and L. S. de Vries, "Diffusion-weighted imaging changes in cerebral watershed distribution following neonatal encephalopathy are not invariably associated with an adverse outcome," *Develop. Med. Child Neurol.*, vol. 55, no. 7, pp. 642–653, Jul. 2013.

[10] F. Pisani and C. Spagnoli, "Monitoring of newborns at high risk for brain injury," *Italian J. Pediatrics*, vol. 42, no. 1, pp. 24–48, Dec. 2016.

[11] S. Ouwehand, L. C. A. Smidt, J. Dudink, M. J. N. L. Benders, L. S. de Vries, F. Groenendaal, and N. E. van der Aa, "Predictors of outcomes in hypoxic-ischemic encephalopathy following hypothermia: A meta-analysis," *Neonatology*, vol. 117, no. 4, pp. 411–427, Apr. 2020.

[12] N. Hayashi-Kurahashi, H. Kidokoro, T. Kubota, K. Maruyama, Y. Kato, T. Kato, J. Natsume, F. Hayakawa, K. Watanabe, and A. Okumura, "EEG for predicting early neurodevelopment in preterm infants: An observational cohort study," *Pediatrics*, vol. 130, no. 4, pp. e891–e897, Jun. 2012.

[13] K. Maruyama, A. Okumura, F. Hayakawa, T. Kato, K. Kuno, and K. Watanabe, "Prognostic value of EEG depression in preterm infants for later development of cerebral palsy," *Neuropediatrics*, vol. 33, no. 3, pp. 133–137, Jun. 2002.

[14] A. Dereymaeker, V. Matic, J. Vervisch, P. J. Cherian, A. H. Ansari, O. De Wel, P. Govaert, M. De Vos, S. Van Huffel, G. Naulaers, and K. Jansen, "Automated EEG background analysis to identify neonates with hypoxic-ischemic encephalopathy treated with hypothermia at risk for adverse outcome: A pilot study," *Pediatrics Neonatol.*, vol. 60, no. 1, pp. 50–58, Feb. 2019.

[15] F. Gao, H. Jia, X. Wu, D. Yu, and Y. Feng, "Altered resting-state EEG microstate parameters and enhanced spatial complexity in male adolescent patients with mild spastic diplegia," *Brain Topogr.*, vol. 30, no. 2, pp. 233–244, Mar. 2017.

[16] F. Gao, X. Wu, Y. Feng, and H. Jia, "Attenuation of temporal correlations of neuronal oscillations in patients with mild spastic diplegia," *Sci. Rep.*, vol. 7, no. 1, p. 14966, Dec. 2017.

[17] S. Sanei and J. A. Chambers, *EEG Signal Processing*. West Sussex, U.K.: Wiley, 2007.

[18] T. Koeda and K. Takeshita, "Electroencephalographic coherence abnormalities in preterm diplegia," *Pediatric Neurol.*, vol. 18, no. 1, pp. 51–56, Jan. 1998.

[19] W. Kułak, W. Sobaniec, and L. Boćkowski, "EEG spectral analysis and coherence in children with hemiparetic cerebral palsy," *Med. Sci. Monitor*, vol. 11, no. 9, pp. 449–455, Sep. 2005.

[20] W. Kulak and W. Sobaniec, "Quantitative EEG analysis in children with hemiparetic cerebral palsy," *NeuroRehabilitation*, vol. 20, no. 2, pp. 75–84, May 2005.

[21] J. N. Saby and P. J. Marshall, "The utility of EEG band power analysis in the study of infancy and early childhood," *Develop. Neuropsychol.*, vol. 37, no. 3, pp. 253–273, Apr. 2012.

[22] F. Sajedi, M. Ahmadlou, R. Vameghi, M. Gharib, and S. Hemmati, "Linear and nonlinear analysis of brain dynamics in children with cerebral palsy," *Res. Develop. Disabilities*, vol. 34, no. 5, pp. 1388–1396, May 2013.

[23] J. M. George, A. M. Pagnozzi, S. Bora, R. N. Boyd, P. B. Colditz, S. E. Rose, R. S. Ware, K. Pannek, J. E. Bursle, J. Fripp, K. Barlow, K. Iyer, S. J. Leishman, and R. L. Jendra, "Prediction of childhood brain outcomes in infants born preterm using neonatal MRI and concurrent clinical biomarkers (PREBO-6): Study protocol for a prospective cohort study," *BMJ Open*, vol. 10, no. 5, May 2020, Art. no. e036480.

[24] T. Takahashi, R. Y. Cho, T. Mizuno, M. Kikuchi, T. Murata, K. Takahashi, and Y. Wada, "Antipsychotics reverse abnormal EEG complexity in drug-Naive schizophrenia: A multiscale entropy analysis," *NeuroImage*, vol. 51, no. 1, pp. 173–182, May 2010.

[25] R. Haartsen, T. BASIS team, E. J. H. Jones, E. V. Orekhova, T. Charman, and M. H. Johnson, "Functional EEG connectivity in infants associates with later restricted and repetitive behaviours in autism; a replication study," *Transl. Psychiatry*, vol. 9, no. 1, p. 66, Dec. 2019.
[26] C. Cans, "Surveillance of cerebral palsy in Europe: A collaboration of cerebral palsy surveys and registers," *Develop. Med. Child Neurol.*, vol. 42, no. 12, p. 816, Feb. 2001.
[27] V. Sakkalis, "Review of advanced techniques for the estimation of brain connectivity measured with EEG/MEG," *Comput. Biol. Med.*, vol. 41, no. 12, pp. 1110–1117, Dec. 2011.
[28] F. Apicella, F. Sicca, R. R. Federico, G. Campatelli, and F. Muratori, "Fusiform gyrus responses to neutral and emotional faces in children with autism spectrum disorders: A high density ERP study," *Behav. Brain Res.*, vol. 251, pp. 155–162, Aug. 2013.
[29] N. E. Huang, Z. Shen, S. R. Long, M. C. Wu, H. H. Shih, Q. Zheng, N.-C. Yen, C. C. Tung, and H. H. Liu, "The empirical mode decomposition and the Hilbert spectrum for nonlinear and non-stationary time series analysis," *Proc. Roy. Soc. London A, Math., Phys. Eng. Sci.*, vol. 454, no. 1971, pp. 903–995, Mar. 1998.
[30] N. Rehman and D. P. Mandic, "Filter bank property of multivariate empirical mode decomposition," *IEEE Trans. Signal Process.*, vol. 59, no. 5, pp. 2421–2426, May 2011.
[31] N. ur Rehman, Y. Xia, and D. P. Mandic, "Application of multivariate empirical mode decomposition for seizure detection in EEG signals," in *Proc. Annu. Int. Conf. IEEE Eng. Med. Biol.*, Aug./Sep. 2010, pp. 1650–1653.
[32] D. Gabor, "Theory of communication. Part 1: The analysis of information," *J. Inst. Electr. Eng., Radio Commun. Eng.*, vol. 93, no. 26, pp. 429–441, Nov. 1946.
[33] S. G. Mallat, "A theory for multiresolution signal decomposition: The wavelet representation," *IEEE Trans. Pattern Anal. Mach. Intell.*, vol. 11, no. 7, pp. 674–693, Jul. 1989.
[34] A. Catarino, O. Churches, S. Baron-Cohen, A. Andrade, and H. Ring, "Atypical EEG complexity in autism spectrum conditions: A multiscale entropy analysis," *Clin. Neurophysiol.*, vol. 122, no. 12, pp. 2375–2383, Dec. 2011.
[35] J. S. Richman and J. R. Moorman, "Physiological time-series analysis using approximate entropy and sample entropy," *Amer. J. Physiol.-Heart Circulatory Physiol.*, vol. 278, no. 6, pp. 2039–2049, Jun. 2000.
[36] S. M. Pincus, "Approximate entropy as a measure of system complexity," *Proc. Nat. Acad. Sci. USA*, vol. 88, no. 6, pp. 2297–2301, Mar. 1991.
[37] M. Tudor, L. Tudor, and K. I. Tudor, "Hans Berger (1873–1941)—The history of electroencephalography," *Acta Med. Croatica*, vol. 59, no. 4, pp. 307–313, 2005.
[38] J. Bruhn, H. Röpcke, and A. Hoeft, "Approximate entropy as an electroencephalographic measure of anesthetic drug effect during desflurane anesthesia," *Anesthesiology*, vol. 92, no. 3, pp. 715–726, Mar. 2000.
[39] C. Bandt and B. Pompe, "Permutation entropy: A natural complexity measure for time series," *Phys. Rev. Lett.*, vol. 88, no. 17, 2002, Art. no. 174102.
[40] E. Olofsen, J. W. Sleigh, A. Dahan, and N. Zealand, "Permutation entropy of the electroencephalogram: A measure of anaesthetic drug effect," *Brit. J. Anaesthesia*, vol. 101, no. 6, pp. 810–821, Dec. 2008.
[41] Y. Bai, Z. Liang, F. Marques, S. De Souza, and G. Antunes, "Cortical entropy changes with general anaesthesia: Theory and experiment," *Physiol. Meas.*, vol. 25, no. 4, pp. 921–934, Aug. 2004.
[42] D. Cui, J. Wang, Z. Bian, Q. Li, L. Wang, and X. Li, "Analysis of entropies based on empirical mode decomposition in amnesic mild cognitive impairment of diabetes mellitus," *J. Innov. Opt. Health Sci.*, vol. 8, no. 5, Sep. 2015, Art. no. 1550010.
[43] R. K. Kana, L. Q. Uddin, T. Kenet, D. Chugani, and R.-A. Muller, "Brain connectivity in autism," *Frontiers Hum. Neurosci.*, vol. 8, no. 7, pp. 8–11, Jun. 2014.
[44] M. Vinck, R. Oostenveld, M. van Wingerden, F. Battaglia, and C. M. A. Pennartz, "An improved index of phase-synchronization for electrophysiological data in the presence of volume-conduction, noise and sample-size bias," *NeuroImage*, vol. 55, no. 4, pp. 1548–1565, Apr. 2011.
[45] Mika. (2010). Brain connectivity toolbox. Mathworks. Accessed: Apr. 20, 2021. [Online]. Available: https://sites.google.com/site/bctnet/
[46] M. Cao, N. Shu, Q. Cao, Y. Wang, and Y. He, "Imaging functional and structural brain connectomics in attention-deficit/hyperactivity disorder," *Mol. Neurobiol.*, vol. 50, no. 3, pp. 1111–1123, Dec. 2014.
[47] A. Zahra, N. Kanwal, N. ur Rehman, S. Ehsan, and K. D. McDonald-Maier, "Seizure detection from EEG signals using multivariate empirical mode decomposition," *Comput. Biol. Med.*, vol. 88, pp. 132–141, Sep. 2017.
[48] M. Hu and H. Liang, "Intrinsic mode entropy based on multivariate empirical mode decomposition and its application to neural data analysis," *Cogn. Neurodyn.*, vol. 5, no. 3, pp. 277–284, Jun. 2011.
[49] E. Theodorsson-Norheim, "Kruskal–Wallis test: BASIC computer program to perform nonparametric one-way analysis of variance and multiple comparisons on ranks of several independent samples," *Comput. Methods Programs Biomed.*, vol. 23, pp. 57–62, Aug. 1986.
[50] Y. Benjamini and Y. Hochberg, "Controlling the false discovery rate: A practical and powerful approach to multiple testing," *J. Roy. Stat. Soc. B, Methodol.*, vol. 57, no. 1, pp. 289–300, 1995.
[51] S. Theodoridis, A. Pikrakis, K. Koutroumbas, and D. Cavouras, *An Introduction to Pattern Recognition: A MATLAB Approach*, 1st ed. Amsterdam, The Netherlands: Elsevier, 2010.
[52] C. Seiffert, T. M. Khoshgoftaar, J. Van Hulse, and A. Napolitano, "RUSBoost: A hybrid approach to alleviating class imbalance," *IEEE Trans. Syst., Man, Cybern. A, Syst., Humans*, vol. 40, no. 1, pp. 185–197, Jan. 2010.
[53] S. Theodoridis, "Classifiers based on Bayes decision theory," in *An Introduction to Pattern Recognition: A MATLAB Approach*. Amsterdam, The Netherlands: Elsevier, 2010, pp. 1–27.
[54] M. Costa, A. L. Goldberger, and C.-K. Peng, "Multiscale entropy analysis of complex physiologic time series," *Phys. Rev. Lett.*, vol. 89, no. 6, p. 68102, Jul. 2002.
[55] C.-K. Peng, M. Costa, and A. L. Goldberger, "Adaptive data analysis of complex fluctuations in physiologic time series," *Adv. Adapt. Data Anal.*, vol. 1, no. 1, pp. 61–70, Jan. 2009.
[56] H. A. Al-Nashash, J. S. Paul, W. C. Ziai, D. F. Hanley, and N. V. Thakor, "Wavelet entropy for subband segmentation of EEG during injury and recovery," *Ann. Biomed. Eng.*, vol. 31, no. 6, pp. 653–658, Jun. 2003.
[57] D. Looney, A. Hemakom, and D. P. Mandic, "Intrinsic multi-scale analysis: A multi-variate empirical mode decomposition framework," *Proc. Roy. Soc. A, Math., Phys. Eng. Sci.*, vol. 471, no. 2173, Jan. 2015, Art. no. 20140709.

DALAL BAKHEET received the master's degree in computer science from King Abdulaziz University, Jeddah, Saudi Arabia, in 2014. She is currently pursuing the Ph.D. degree in computer science with the University of Southampton, Southampton, U.K. Her research interests include the brain–computer interface, neurodevelopmental disorders, brain signal processing, and biomedical engineering.

NOURA ALOTAIBI is currently pursuing the Ph.D. degree in computer science with the University of Southampton, Southampton, U.K. Her research interests include biomedical signal processing, neural engineering, brain–computer interface, and machine learning.

DANIEL KONN is currently a Consultant Clinical Neurophysiologist. His research interests include single-fibre EMG to assess neuromuscular junction dysfunction, prolonged EEG, including ambulatory EEG and videotelemetry. He has also gained in-depth knowledge and experience in pediatric and neonatal EEG.

BRIGITTE VOLLMER is currently an Associate Professor of neonatal and pediatric neurology. Her research interests include neonatal neurology, neurodevelopment, and neuroimaging.

KOUSHIK MAHARATNA (Member, IEEE) received the Ph.D. degree from Jadavpur University, Kolkata, India, in 2002. From 2000 to 2003, he was a Research Scientist with Innovations for High Performance, Frankfurt (Oder), Germany. He joined the Department of Electrical and Electronic Engineering, University of Bristol, Bristol, U.K., as a Lecturer, in 2003. Since 2006, he has been with the School of Electronics and Computer Science, University of Southampton, Southampton, U.K., where he is currently a Professor. His current research interests include biomedical signal processing, next generation healthcare systems development, and very large scale integration design for signal processing systems.